Flow Turbulence Combust (2015) 94:323–338
DOI 10.1007/s10494-014-9572-2

Investigation of Glycerol Atomization in the Near-Field of a Flow-Blurring Injector using Time-Resolved PIV and High-Speed Visualization

Lulin Jiang · Ajay K. Agrawal

Received: 3 June 2014 / Accepted: 2 October 2014 / Published online: 21 October 2014

Abstract Glycerol has very high kinematic viscosity and high vaporization and auto-ignition temperatures, but it has been effectively atomized at room temperature by using a novel flow blurring (FB) injector and then cleanly combusted without any combustor hardware modification. The present study qualitatively and quantitatively reveals the details of glycerol atomization in the near field of the FB injector. Time-resolved Particle Image Velocimetry (PIV) with exposure time of 150 ns and image pair acquisition rate of 15 kHz is utilized to probe the glycerol spray at spatial resolution of 16.83 μm per pixel. PIV results describe the droplet dynamics in terms of instantaneous, mean, and root-mean-square (RMS) profiles of the axial velocity. In addition, high-speed imaging (75 kHz) coupled with backside lighting is applied to reveal the glycerol breakup process at spatial resolution of 7.16 μm per pixel and exposure time of 1 μs. Results indicate that the primary breakup by FB atomization or bubble explosions occurs inside the injector and it results in ligaments and droplets at the injector exit. Then, the secondary breakup by Rayleigh-Taylor instability occurs in the near-field of the injector exit where the high-velocity atomizing air stretches the ligaments into thin ligaments that disintegrate into smaller ligaments, and subsequently, into droplets. Thus, within a short distance downstream of the injector exit (<30 mm), most of the glycerol is atomized into fine droplets demonstrating excellent atomization performance of the FB injector.

Keywords Spray and droplet combustion · Fuel atomization · Glycerol · Time-resolved PIV · High-speed flow visualization

L. Jiang · A. K. Agrawal (✉)
Department of Mechanical Engineering, The University of Alabama, Box 870276, Tuscaloosa, AL 35487-0276, USA
e-mail: aagrawal@eng.ua.edu

L. Jiang
e-mail: ljiang5@crimson.ua.edu

1 Introduction

1.1 Glycerol production, atomization and combustion

Liquid fuel combustion is one of the main ways to supply the energy needs of our modern world. However, recent concerns with conventional fossil fuel resources have prompted combustion researchers to seek effective ways to utilize liquid fuels without harming the environment [1–4]. Concurrently, researchers are exploring renewable and alternative fuels to fulfil the increasing energy demand [5]. For example, biodiesel is a promising alternative fuel because its thermo-physical properties are similar to those of the diesel fuel [6–10]. However, large surpluses of the extremely viscous glycerol having high vaporization and auto-ignition temperatures are produced as the unintended by-product of the biodiesel production [10–12]. Many biodiesel producers generally dispose glycerol as waste product even though it has moderate low heating value of about 16 MJ/kg [11]. Thus, in recent years, research has focused on direct combustion of glycerol, but achieving low emissions has been challenging [10–15].

Effective atomization of liquid fuels plays a major role on fuel vaporization and fuel-air mixing processes in the injector near field and hence, on clean combustion by approaching premixed conditions to minimize nitric oxide (NO_x), carbon monoxide (CO), and soot emissions [16–18]. For continuous flow applications, typically air-assist or air blast (AB) injectors are used to atomize the fuel by relying upon the shear layer instabilities created between the fuel jet and the atomizing air [19–21]. However, shear layer instabilities are suppressed by the high viscosity of the liquid jet which makes it difficult to atomize liquids such as glycerol [19, 20]. In previous studies with AB injectors, glycerol was preheated to reduce its kinematic viscosity and the preheated glycerol was burned with preheated combustion air, which requires additional energy input and adversely affects the overall efficiency [10, 11, 14, 15]. Another mechanism called effervescent atomization (EA) uses a two-phase flow concept to overcome the limitation of AB injectors for viscous liquids. In EA, pressurized air is introduced into the liquid through pores on the surface of a mixing chamber to form a two-phase mixture farther upstream of the injector body. The two-phase mixture flows through the injector and causes the gas bubbles to burst at the injector exit where the pressure decreases suddenly. The surrounding liquid is therefore broken into ligaments and droplets during the bubble explosions [22]. The internal two-phase flow regime in the mixing chamber might transit from bubbly flow to slug flow with gas voids (i.e. large bubbles) or annular flow with no bubbles resulting in pulsations [22]. The two-phase flow instabilities and the requirement of high pressure atomizing air have limited widespread application of effervescent atomization [22].

1.2 Flow-blurring (FB) injection

Previous studies by our research group have shown extremely low emissions of CO and NO_x for combustion of diesel, biodiesel, straight vegetable oil (VO) and even glycerol without preheating either the fuel or the combustion air by using a novel flow-blurring (FB) injector [16, 17, 20, 24, 25]. The clean blue visual flames obtained for all of these fuels demonstrated the superior fuel flexibility of the FB injector [16, 17, 20, 24, 25]. As reported first by Gañán-Calvo [26], in the FB injector, the atomizing gas bifurcates at the stagnation plane developed aerodynamically in the annular gap between the liquid tube tip and the injector orifice. A portion of the gas flow entrains into the liquid supply tube while the rest exit through the injector orifice. Consequently, two-phase mixture is formed at the tip of the

liquid supply tube inside the FB injector as shown in Fig. 1. Formation of the two-phase mixture in the FB injector is fundamentally different from the forced two-phase mixing in the upstream mixing tube of the EA injector, which requires very high pressure gas and the long residence time for the two-phase flow through the injector causes combustion instabilities. The aerodynamic requirements to form the two-phase flow in the FB atomizer are (1) the inside diameter, D, of liquid tube must be equal to that of the injector orifice, and (2) the gap, between the liquid supply tube tip and the injector orifice must be less than or equal to $0.25D$. The atomizing gas bubbles expand and burst near the injector orifice resulting in primary breakup of the surrounding liquid (see Fig. 1), as documented by the internal flow visualization of a transparent FB injector operated with water and air [27]. Gañán-Calvo [26] used low viscosity fluids, water and ethanol, to discover the FB atomization. Later, our research group has used the Phase Doppler Particle Analyser (PDPA) technique to measure droplet diameter distributions and to quantify the average mass flow-weighted Sauter Mean Diameter (SMD) at locations 20 mm and 100 mm downstream of the injector exit, respectively for straight VO and glycerol [20, 24, 28, 29]. Results showed mass flow-weighted SMD of 30 to 40 μm for both VO and pure glycerol for given mass flow rates of fuel and atomizing air, indicating that unlike a typical AB injector, the FB injector is less sensitive to the physical properties of the liquid. For given liquid and atomizing air flow rates, the FB injector produces sprays with finer droplets and with less pressure drop across the injector than an AB injector [20, 28, 29].

1.3 Motivation of the present study

Previous studies have reported PDPA measurements of droplet diameter distributions in sprays of diesel, VO, and glycerol at locations farther downstream of the injector exit [21, 24]. However, an investigation of the spray features near the injector exit is necessary to fully understand the atomization processes in the FB injector; note that such information is difficult to obtain for a typical AB injector because it produces an optically inaccessible liquid jet core at the injector exit. Recently, we have investigated the FB injector near field of water spray for air to liquid mass ratio (ALR) of 2.0 [30]. Results reveal that most of water at the injector exit has been atomized into droplets. The maximum variations in the droplet diameter occurred at the periphery closer to the injector exit where larger droplets with

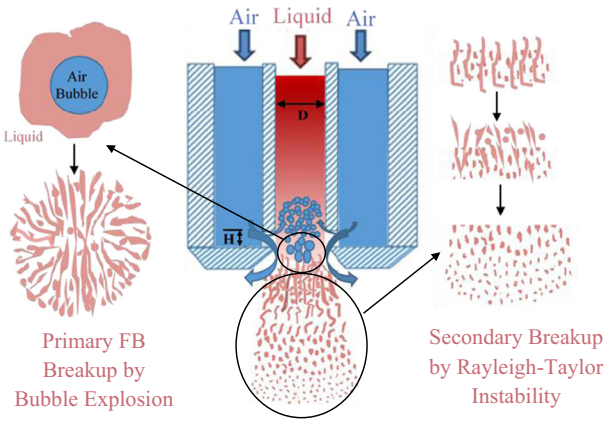

Fig. 1 Working principle of the FB injector

diameter ranging between 20 μm and 100 μm appeared occasionally, but they disintegrated into smaller droplets at downstream locations [30]. Considering the increasing interest in clean combustion of highly viscous liquid fuels, a FB injector is used in this study to atomize pure glycerol with the goal to identify the atomization mechanisms and thus, delineate the spray characteristics near the injector exit. Time-resolved Particle Image Velocimetry (PIV) technique is used to acquire the velocity measurements, with atomized liquid serving as the seed particles. In addition, high-speed flow visualization with backside lighting is employed to identify the important features of glycerol atomization in the near field of the FB injector at a high spatial resolution.

2 Experimental Setup

Figure 2 shows the schematic of the FB injection system setup. The inside diameter, D, of the liquid supply tube as well as that of the injector orifice is 1.5 mm. The gap between the liquid supply tube tip and injector orifice, $H = 0.375$ mm is used to create two-phase mixture at the tip of the liquid supply tube. Glycerol is pumped by a Cole Parmer high performance peristaltic metering pump (Model 7523-40) with an accuracy of ±0.25 % of the reading and it enters the injector holder from the side and flows into the injector connected with the holder. Atomizing air (AA) is introduced from the upstream of the injector holder, and its flow rate is measured by an Aalborg mass flow meter (Model CFM47) with an accuracy of ±1.5 % of the reading. Atomizing air and glycerol flow rates are 20 standard litres per minute (slpm) and 9.5 ml/min, respectively, yielding atomizing air to liquid ratio (ALR) by mass of 2.0. Based on the measured air mass flow rate , the average axial velocity of the atomizing air at the injector exit is about 127 m/s.

The time-resolved PIV technique is used to quantify the movement of atomized glycerol parts in the near injector region by computing the instantaneous velocity field of glycerol droplets and/or ligaments. A dual head Nd: YAG laser (Quantronix Hawk-Duo 532-12-M laser with the wave length of 532 nm and average power of 120 W) is used to gener-

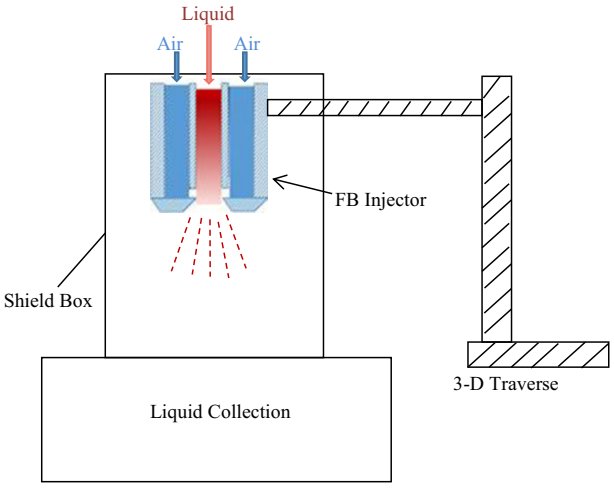

Fig. 2 Schematic of the FB injector experimental setup

ate two laser pulses each with pulse duration of about 150 ns which is also the exposure time in the camera images. Note that a glycerol part moving with the velocity of 100 m/s will travel 15 μm or less than one pixel during the laser pulse duration of 150 ns, and thus, the glycerol movement in the PIV images can be assumed to be nearly frozen. TSI divergent sheet optics with -15 mm focal-length cylindrical lens and 1000 mm spherical lens is used to generate 1 mm thick laser sheet to illuminate the glycerol spray. A high speed camera (Photron FASTCAM SA5) with a microscopic lens set perpendicularly focuses on the laser sheet with the field of view (FOV) of 7.0 mm × 7.0 mm providing spatial resolution of 16.83 μm per pixel verified by using a calibration target with a rectangular grid. The camera is synchronized with the laser pulse setting to acquire frame-straddle image pairs at interval of 1 μs and repetition rate of 15 kHz. The PIV system is capable of detecting particles with the diameter of $1/10^{th}$ pixel, i.e. 1.7 μm.

The instantaneous velocity field is computed using TSI Insight software (version 4.0) with the cross-correlated sub-regions of every image pair acquired at 1 μs time interval. The initial interrogation window size of 64 × 64 pixels with 50 % overlap spacing is used to calculate the velocity vectors. This window size is small enough to minimize the measurement noise but still include more than 10 particle pairs, ensuring 100 % valid detection [31]. Considering the out-of-plane displacement, the present setup gives about 90 % of particle pairs in the interrogation spot, that is, about 10 % pairs are lost due to out-of-plane motion. Thus, there are more than 10 paired particles remaining in the analysed window, ensuring accuracy of the results. Spurious vectors are eliminated using local median test, a range filter, and a signal to noise ratio (SNR) filter. In the local median test, the vector is rejected and replaced by a valid secondary peak when the difference between the current velocity vector and the local median velocity of neighbouring vectors exceeds the given tolerance (two times of the local median value). A range filter is applied to filter out the vector exceeding reasonable limits in the axial (V) and radial (U) displacements. A vector is valid when the SNR is greater than 1.4. A recursive filling procedure is used to fill the holes by employing the local mean in the vector field passed through the median test and the two validation filters. The holes are first filled with the most valid neighbouring vectors and then the ones with the second most valid neighbours. Note that the Phase Doppler Particle Analyzer (PDPA) is unable to measure the glycerol spray in the injector near field. Therefore, the PIV technique is used to measure the droplet/ligament velocity which is inversely related to the diameter. However, the droplet diameter distribution cannot be measured directly by the present PIV setup.

PIV measurements are supplemented with high-speed imaging combined with backside lighting to visualize the glycerol atomization near the injector exit at high spatial resolution. A very high intensity white light source produced by laser-driven plasma (Energetiq LDLS) is used as the backlight to illuminate the view area. A high-speed camera (Photron FASTCAM SA5), mounted with 100 mm focal-length lens, a 2× lens extender, and 130 mm length of extension tubes captures the visual glycerol spray images in the FOV of 1.8 mm × 2.0 mm at spatial resolution of 7.16 μm per pixel, framing rate of 75 kHz, and exposure time of 1 μs (the limit of the camera) to minimize the blurring caused by the motion of the atomized glycerol. Note that, the exposure time for visualization experiments is 6.7 times greater than the laser pulse duration, and thus, the fast moving glycerol droplets can blur the images. Furthermore, the backlight is much less intense than the laser in the PIV measurements, which precludes the visualization of small droplets. Still, visualization images offer qualitative details, and a rough estimate of the size of the droplets/ligaments that are at least two pixels wide, i.e. 15 μm.

3 Results and Discussions

3.1 PIV measurements and analysis

Figure 3a-b show glycerol images at the injector exit acquired using time-resolved PIV. The flow direction is downwards, the field of view is 7.0 mm × 7.0 mm, and the spatial resolution is 16.83 μm per pixel. Figure 3c shows the computed instantaneous velocity vector field obtained from the image pair of Fig. 3a-b taken at 1 μs interval. In Fig. 3a-b, glycerol droplets and ligaments denoted by the brighter thick and thin lines appear at the injector exit, i.e., at the top of the image. Evidently, these structures represent shattered glycerol from the explosion of air bubbles referred to as the primary breakup by FB atomization [19]. Interestingly, bubble explosions cannot be seen in the PIV images, suggesting that the primary breakup by the FB atomization takes place upstream, i.e., in-between the injector orifice and injector exit as illustrated in Fig. 1. In both PIV images, ligaments are observed near the injector exit, but they breakup at downstream locations, evidently by Rayleigh-Taylor instabilities resulting from a slow-moving, dense fluid (glycerol) being accelerated by a fast moving light fluid (atomizing air); the average axial velocity of the atomizing air at the injector exit (127 m/s) is much greater than the glycerol drop/ligament velocity as discussed in the next section. In summary, the atomization process involves two distinct mechanisms illustrated in Fig. 1: (a) the primary breakup by the FB atomization (or bubble explosions) inside the injector, and (b) the secondary breakup near the injector exit by the Rayleigh-Taylor instabilities. The absence of a liquid core in the PIV images vividly illustrates the superior capability of the FB injector to effectively atomize an extremely high viscosity liquid. The instantaneous velocity vectors in Fig. 3c indicate higher velocity at locations where droplets are present and relatively lower velocities at positions where ligaments are located. This result signifies that the glycerol droplets move at higher velocities to more closely follow the atomizing air flow, while the glycerol ligaments travel at lower velocities until they breakup into droplets. That is, the velocity of the droplet/ligaments is inversely proportional to their size although the precise relationship remains unknown.

Temporal analysis In this section, PIV measurements of instantaneous axial velocity of droplets/ligaments are analyzed at the spray centre (x = 0.0 mm) and periphery (x = -1.50 mm) for axial planes, y = 0.35 mm, 2.25 mm, 3.75 mm, and 6.80 mm using 750 consecutive data points for a time span of 50 ms. Figure 4 shows that the axial velocity at

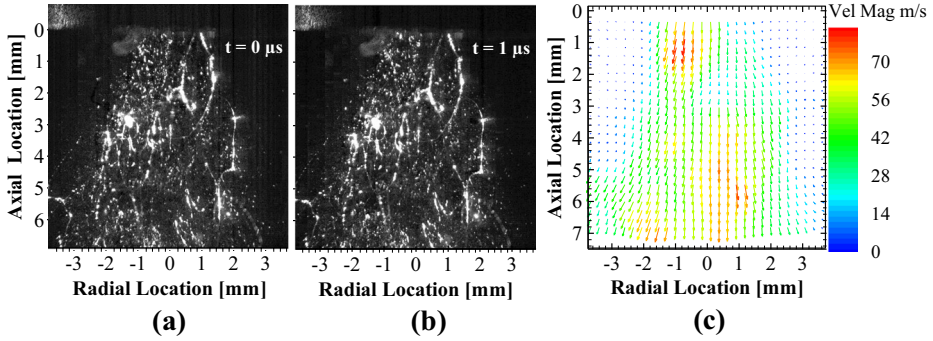

Fig. 3 PIV image pair of the glycerol spray **a**-**b**, and the corresponding velocity vectors **c**

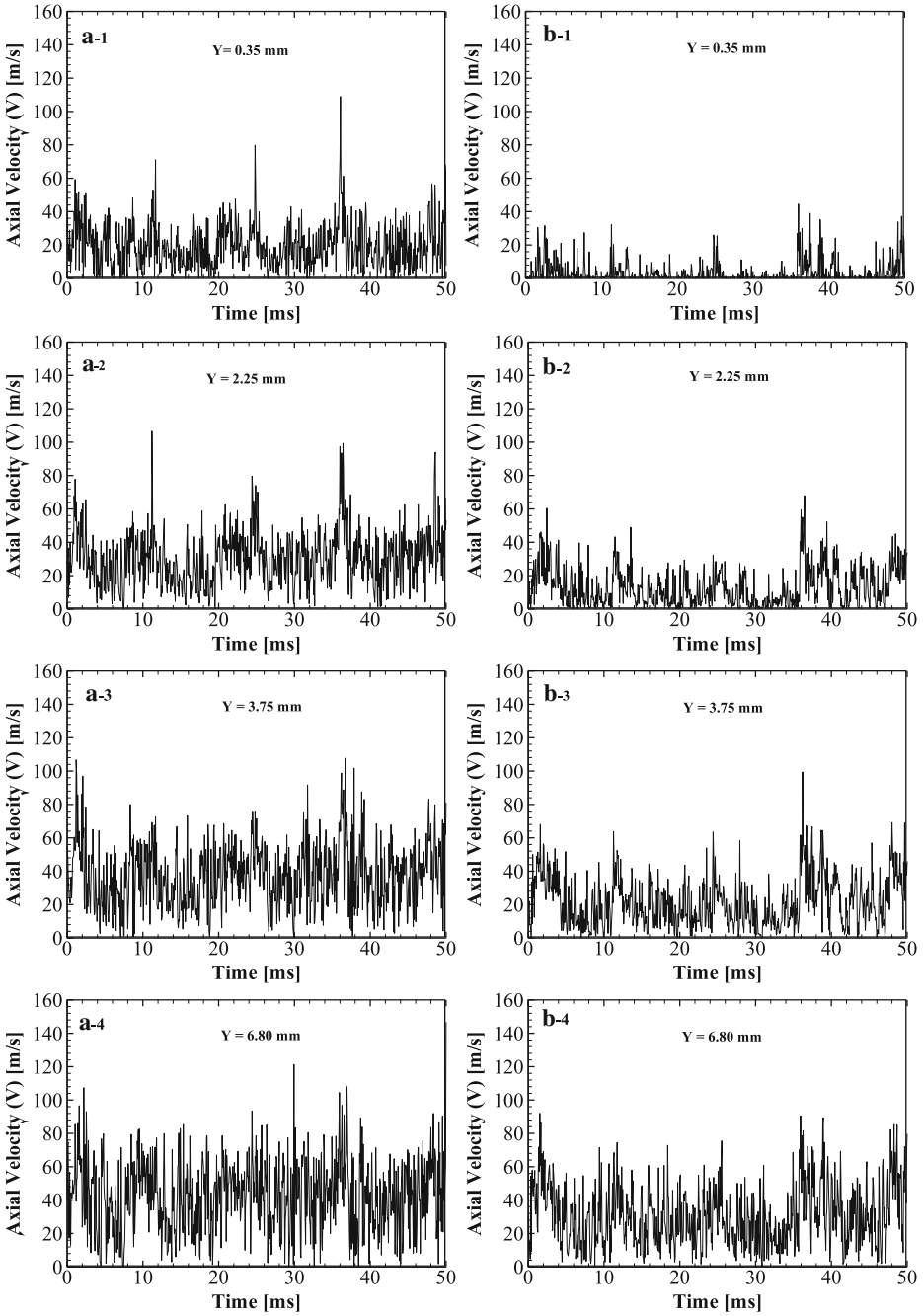

Fig. 4 Time analysis of axial velocity for ALR = 2.0 at **a** X = 0.00 mm and **b** X = -1.50 mm

the spray centre near the injector exit (y = 0.35 mm) varies generally between 10 and 40 m/s, although occasional peaks of about 70 to 110 m/s are also present. Results in Fig. 4 suggest that the FB atomization produces mostly ligaments and few droplets at the centre of the injector exit. At the periphery, the axial velocity is generally less than 20 m/s with occasional occurrences of 30 to 40 m/s. Thus, the FB atomization produces more ligaments at the spray periphery as compared to the spray centre, a finding which is consistent with the PIV images in Fig. 3a-b.

Downstream at y = 2.25 mm, the axial velocity increases to 10 to 50 m/s with occasional high peaks of around 80 to 110 m/s at the spray centre and to 0 to 30 m/s with occasional peaks of 40 to 60 m/s at the spray periphery. An increase in the axial velocity signifies breakup of droplets and/or thinning of ligaments by momentum transfer from the atomizing air flow at a higher velocity. The above trend continues at farther downstream locations of y = 3.75 mm and 6.80 mm. In each case, the axial velocity increases with the increasing distance from the injector exit. For example, at y = 3.75 mm, the axial velocity range at the spray centre and periphery is 10 to 60 m/s and 5 to 40 m/s, respectively. Similarly, at y = 6.80 mm, the axial velocity range at the spray centre and periphery is 20 to 80 m/s and 5 to 60 m/s, respectively. The consistent increase in the axial velocity of glycerol ligaments/droplets signifies acceleration and secondary atomization throughout the field of view, i.e., between y = 0.0 and 6.80 mm. Conversely, the average velocity of the atomizing air is expected to decrease in the flow direction from its highest value of 127 m/s at the injector exit.

Next, the Weber (We) number for the present flow conditions is estimated from Eq. 1 to estimate and quantify the secondary atomization by Rayleigh-Taylor instabilities [32–36]:

$$We = \frac{\rho_g U_{rel^d}^z}{\sigma} \tag{1}$$

where $\rho_g$is the gas phase density (kg/m^3); U_{rel} is the relative velocity (m/s), i.e. the velocity difference between the atomizing air and liquid, d is the droplet diameter or ligament thickness and σ is the surface tension (N/m) of the liquid. Weber number signifies the ratio of the inertial force of the atomizing air to the surface tension force of the liquid [32–36]. High Weber number signifies that the inertial force can overcome the surface tension force to result in liquid breakup by the secondary atomization. In the present study, the average atomizing air velocity (at the injector exit) is about 127 m/s and atomized glycerol velocity varies generally between 0 and 60 m/s (see Fig. 4), which yields the relative velocity (U_{rel}) of approximately 70 to 125 m/s. For observed droplet diameter or ligament thickness range of around 20 to 100 μm, the estimated Weber number of glycerol spray in the near field of the injector varies between 2.3 and 27.0. Note that the air velocity is the highest at the injector exit and it would decreases in the flow direction, while the reverse is true for the liquid phase. Thus, the relative velocity and hence the Weber number is the highest at the injector exit, and it gradually decreases in the flow direction.

Probability distribution Next, the probability distribution of ligament/droplet axial velocity at different locations is presented in Fig. 5 at the chosen axial locations for two transverse positions; spray centre (X = 0.00 mm) and spray periphery (X = -1.50 mm). At the injector exit, the probability is the highest for the axial velocity between 15 m/s and 25 m/s at the centre and about 15 m/s at the periphery. PIV images in Fig. 3 show that mostly ligaments are observed at these locations. Few droplets are also present at the centre, and thus, it would be reasonable to assume that axial velocities of <25 m/s represent ligaments and axial velocities of >55 m/s signify droplets, while the in-between velocities could represent either ligaments or droplets. At the spray centre, Fig. 5a-b show that with increasing axial

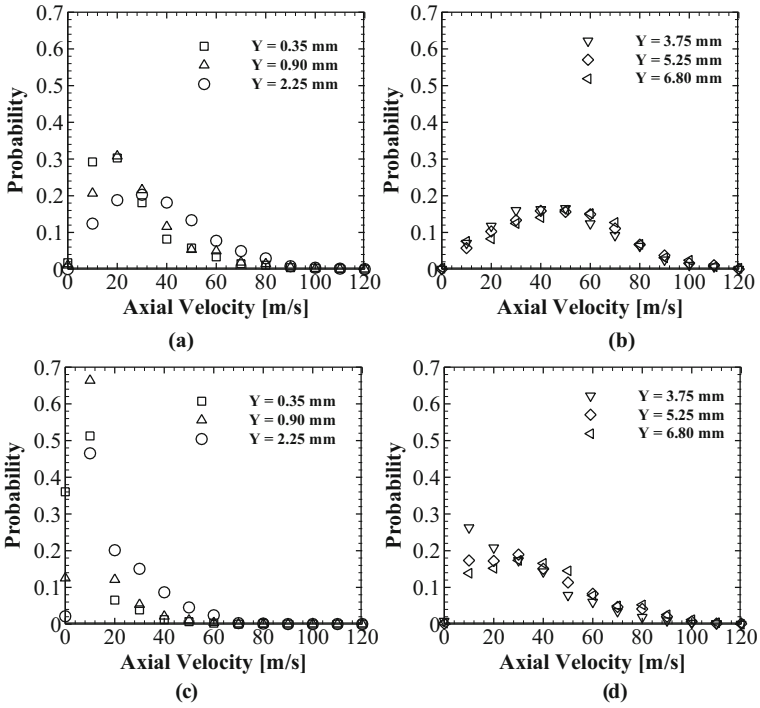

Fig. 5 Probability distribution plots of axial velocity at various axial locations; X = 0.00 mm in **a** and **b**, and X = - 1.50 mm in **c** and **d**

coordinate, the probability curves shift towards higher axial velocities. The axial velocity is less than 25 m/s for 60 %, 30 %, 20 %, and 20 % of the times respectively at Y = 0.35 mm, 2.25 mm, 3.75 mm, and 6.80 mm, indicating fewer ligaments downstream of the injector exit. Similarly, the axial velocity is greater than 55 m/s for 10 %, 25 %, 50 %, and 50 % of the times respectively at Y = 0.35 mm, 2.25 mm, 3.75 mm, and 6.80 mm. This shift toward higher axial velocities signifies acceleration of the liquid by the gas phase undergoing deceleration. The Rayleigh-Taylor instabilities in this process breakup the ligaments/droplets as observed in the PIV images in Fig. 3. The shift towards higher velocities is most significant at the injector exit (Y <= 2.25 mm), and it gradually decreases in the flow direction. Again, this result signifies a decrease in the relative velocity and hence in the Weber number in the flow direction. Similar trends are observed at the spray periphery as shown in Fig. 5c-d. However, at each axial location, the probability distribution curves at the periphery are biased towards lower velocities compared to those at the centre, indicating that more ligaments (or fewer droplets) are present away from the spray centre.

Time-averaged and root-mean square axial velocities Figure 6 shows the time-averaged velocity vectors calculated from instantaneous velocity fields of glycerol droplets/streaks obtained from 1500 frame-straddle PIV image pairs. Every instantaneous vector field is computed from the image pair acquired with the time interval of 1 μs, which is much less than the time needed for secondary breakup of glycerol droplets/ligaments, visually revealed by the striking similarity of the image pair in Fig. 3a and b. Figure 6a shows that the average velocity of droplets/ligaments increases in the flow direction and decreases from the spray

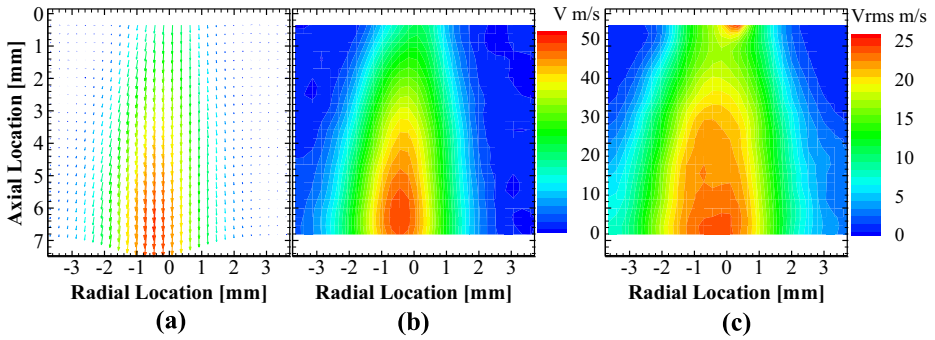

Fig. 6 Time-averaged field: **a** velocity vectors, **b** axial velocity, and **c** RMS axial velocity

centre to the periphery. The increase in the average droplet/ligament velocity in the flow direction signifies acceleration of the liquid phase by the gas phase which itself is decelerating according to the momentum conservation principle. The average axial velocity contour in Fig. 6b quantitatively depicts the details of the ligament/droplet movement. For every axial plane, the average axial velocity is highest at the spray centre and it decreases in the radial direction. The radial extent of the spray increases in the flow direction which is a typical feature of the jet flows. The velocity vectors in Fig. 6a indicate that the axial velocity is the dominant component in the spray.

Next, root mean square (RMS) velocities of ligaments/droplets are computed to quantitatively characterize the FB spray at the injector exit. Note that the RMS velocity can be related to the fluctuations in the size of glycerol droplets and/or ligaments. Figure 6c shows contour of RMS axial velocity of glycerol droplets/ligaments. It reveals high RMS axial velocity at the injector exit caused by the FB atomization by air bubble explosions inside the injector breaking glycerol into ligaments and droplets. RMS axial velocity decreases in the flow direction indicating smaller change in the size of glycerol ligaments/droplets between axial locations, Y = 0.00 mm and 2.00 mm, where Y = 0.00 mm represents the injector exit. Subsequently, the RMS axial velocity increases in the flow direction between Y = 2.00 mm and 7.00 mm, signifying an increased tendency for the liquid breakup in this region by the Rayleigh-Taylor instabilities. Figure 7a shows the radial profiles of ligament/droplet axial velocity at several axial planes. Again, the axial velocity increases in the flow direction as glycerol disintegrates into smaller particles that tend to streamline with the atomizing airflow. In Fig. 7b the increase in the RMS axial velocity signifies the increasing importance of the secondary breakup in the centre region of the spray between y = 2.00 mm and 6.80 mm.

In general, PIV results demonstrate that glycerol ligaments and droplets, rather than jet core typically observed for an AB injector, appear immediately at the FB injector exit because of the primary breakup within the FB injector. Glycerol ligaments move slowly and interact with the high-velocity atomizing air to gradually disintegrate into droplets by the Rayleigh-Taylor instabilities. This secondary breakup process is efficient but still present at the end of the FOV, i.e., Y = 6.80 mm, where ligaments moving at velocities of less than 25 m/s are present at the spray centre for about 20 % of the times. PIV experiments visually and quantitatively shows the excellent performance of the FB injector to atomize a liquid with extremely high kinematic viscosity.

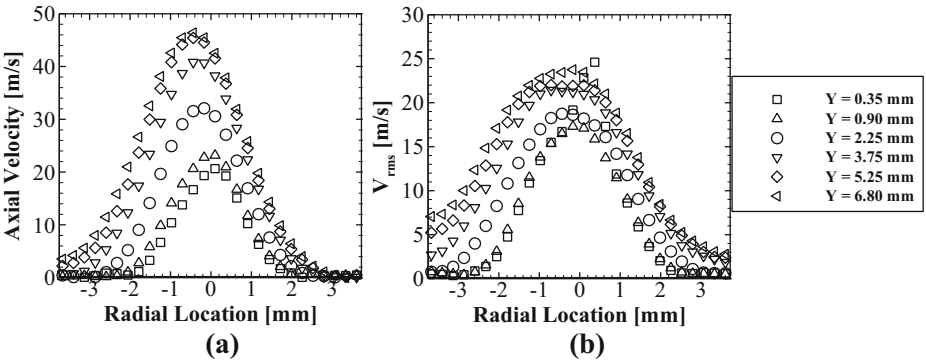

Fig. 7 Radial profiles of time-average **a** axial velocity, and **b** RMS axial velocity

3.2 High-speed flow visualization

The PIV measurements are complimented with high-speed imaging of glycerol atomization in the injector near field. Figure 8 shows the images of atomized glycerol parts at several FOVs in the axial direction, each with view area of 1.8 mm × 2.0 mm and spatial resolution of 7.16 μm per pixel. The images in Fig. 8 cover the axial distance Y = 0.00 mm to 34.00 mm, and the image FOVs are chosen to represent the obvious variations in the glycerol parts. Note that small droplets cannot be individually identified in these images because of the light intensity and camera exposure time limitations as discussed previously. Unlike the powerful laser in PIV measurements, the backlight for imaging experiments cannot illuminate the small droplets. Further, fast-moving small droplets frozen in the PIV images during the laser pulse duration of about 150 ns cause blurring for the exposure time of 1 μs of the high-speed camera. Thus, only ligaments and large droplets that are at least two pixels in size (or 15 μm) can be resolved in the visualization images.

Based on the visual images, the secondary atomization of glycerol ligaments/droplets by Rayleigh-Taylor instabilities is found to undergo four stages. In the first stage, the primary breakup by FB atomization or bubble explosion within the injector results in ligaments and droplets at the injector exit (see Fig. 8a), which is consistent with the PIV images and analysis. The thickness of the ligaments ranges from about 20 μm marked as B to around 35 μm marked as A in Fig. 8a, while most of the ligaments are around 35 μm thick. In the second stage between Y = 2.00 mm to 12.00 mm, ligaments interact with the high-velocity atomizing air and intermingle with one another as illustrated in Fig. 8b. The ligament thickness ranges from approximately 20 μm marked by D to about 28 μm depicted as C. The majority of the ligaments in this region are about 28 μm thick, indicating significant thinning by shearing from the atomizing air. Thin ligaments breakup in the third stage between Y = 12.00 mm to 28.00 mm as shown in Fig. 8c. The long ligaments observed previously breakup into shorter ligaments with the thickness of about 25 μm shown as E in the image. Shorter ligaments with such small thickness further deform to produce small droplets with the diameter of about 21 μm marked by F in the image. Figure 8d depicts the fourth stage, for Y = 28.00 mm to 32.00 mm, where most of the glycerol ligaments are broken into small droplets, with diameter of about 21 μm marked by G. Few relatively large droplets, up to about 70 μm in diameter marked by H, occasionally appear at this location although they are produced at the injector exit by FB atomization. Note that, the size of the ligaments

and droplets reported here are approximate values. The images show that both the primary atomization within the FB injector and the secondary atomization in the injector near field are important mechanisms to produce the glycerol spray. In a combustion environment, the secondary atomization of glycerol will further improve because of the interaction with the combustion air, in addition to the atomizing air passing through the injector. In previous studies, the flame of glycerol atomized by the same FB injector was stabilized at around Y = 70 mm [24, 37] and it resulted in clean combustion, which can be explained by the fine glycerol spray produced in the near field (within Y = 35 mm) of the FB injector.

Figure 9 shows the consecutive images with the time interval of 1/75000 s to reveal the disintegration of longer ligaments into shorter, thinner ligaments by the fast-moving atomizing air. Glycerol ligaments generated from the primary breakup by the FB atomization inside

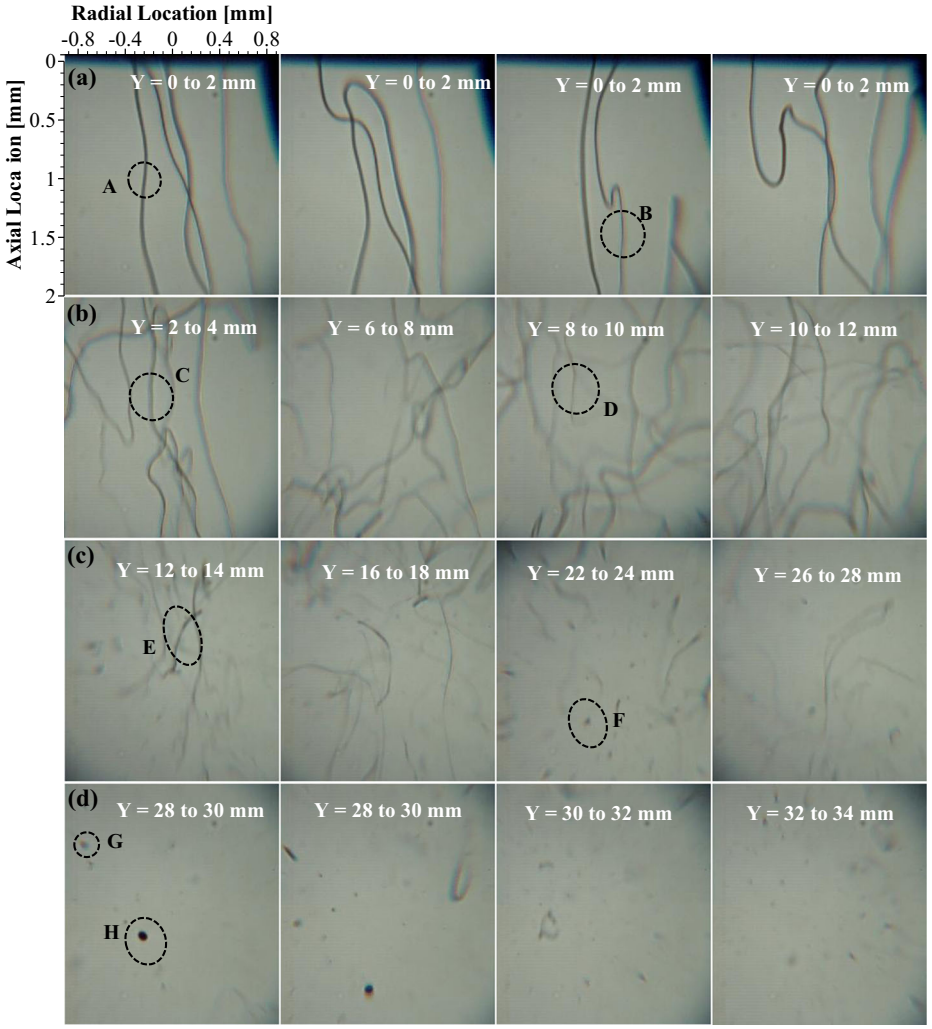

Fig. 8 Flow visualization in the FOV of 1.8 mm x 2.0 mm for **a** Y = 0 - 2 mm, **b** Y = 2 - 12 mm, **c** Y = 12 - 28 mm, and **d** Y = 28 - 34 mm

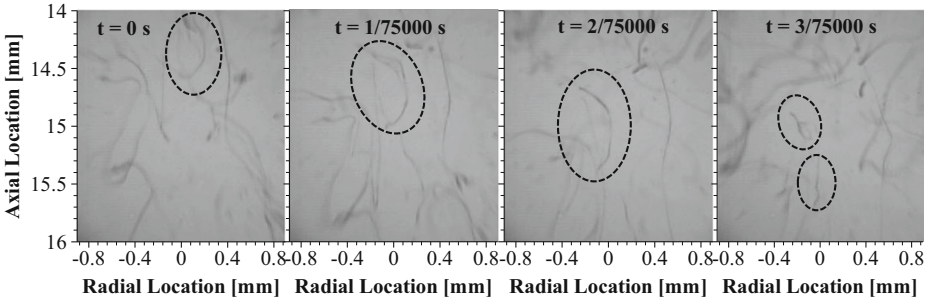

Fig. 9 Image sequence illustrating breakup of long streaks into short streaks with the time interval of 1/75000 s in the FOV of 1.8 mm × 2.0 mm

the injector undergo interweaving and thinning during the first two stages of the secondary atomization process shown in Fig. 8. Relatively thinner ligaments quickly deform and disintegrate into shorter ligaments within 2 mm downstream of the injector exit, as shown in Fig. 9, by the Rayleigh-Taylor instabilities. Sequential images in Fig. 10 illustrate the gradual breakdown of short ligaments into small droplets in the fourth stage of the secondary atomization process. Short ligaments rotate and decompose into droplets as they interact with the injected high-velocity atomizing air, indicating that the FB atomizer quickly produces fine glycerol spray in the near field of the injector. The secondary breakup is visually observable during the time interval of 13.3 μs between the images in Figs. 9 and 10. Thus, the time interval of 1 μs between PIV image pairs is adequate to capture the instantaneous velocity field without interfering with the deformation and secondary breakup processes. Images in Figs. 9 and 10 provide visual details of the atomization process which cannot be deciphered from the PIV images acquired with larger spatial resolution and smaller framing rate.

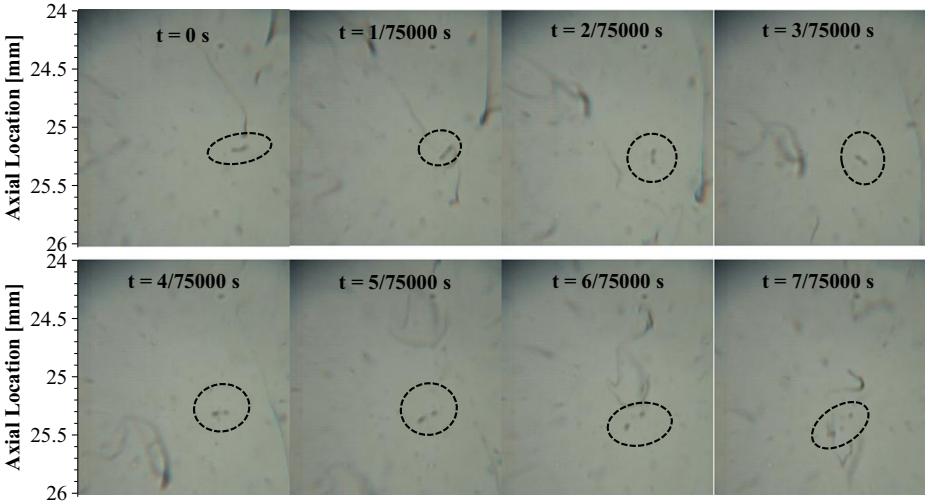

Fig. 10 Image sequence illustrating breakup of short streaks into droplets with the time interval of 1/75000 s in the FOV of 1.8 mm × 2.0 mm

In general, the primary breakup by the FB atomization produces ligaments and droplets of glycerol at the injector exit. Initially, the glycerol ligaments are about 40 μm thick, but they undergo thinning and breaking into small ligaments and then breakup into small droplets by the high-velocity atomizing air undergoing deceleration. At Y = 28 mm, most of the ligaments are atomized into fine droplets, with diameter of around 21 μm, indicating the great capability of the FB injector to effectively atomize extremely viscous glycerol. In a practical swirl-stabilized combustor, the primary airflow would further improve the secondary atomization and hence, even smaller droplets can be expected to facilitate premixed, low-emission combustion of glycerol and other highly viscous fuels.

4 Conclusions

Glycerol atomization by the FB injector is investigated in detail using time-resolved PIV and high-speed flow visualization techniques. PIV images clearly show that both glycerol ligaments and droplets are formed at the injector exit by the primary atomization inside the FB injector. The instantaneous velocity field reveals that the glycerol droplets move faster to follow the high-velocity injected air while the ligaments move slower to eventually breakup at downstream locations. Temporal analysis and probability distribution profiles of axial velocity at various locations substantiate the existence of ligaments and droplets at the injector exit and an increasing numbers of faster moving droplets at downstream locations. The axial velocity of the liquid phase increases in the flow direction signifying breakup of the ligaments or droplets by the Rayleigh-Taylor instabilities. RMS axial velocity of the liquid phase increases in the center region at downstream locations where secondary breakup is prominent. Overall, the glycerol atomization occurs in four stages: (1) formation of thick ligaments and relatively larger droplets at the injector exit resulting from the primary breakup by the FB atomization inside the injector, (2) thinning of ligaments as they intermingle and interact with the high-velocity atomizing air, (3) breakup of the most of the ligaments into smaller ligament and droplets, and (4) breakup of the droplets and remaining ligaments into small droplets with diameter of around 21 μm. In all of these four stages, most of the glycerol ligaments and droplets have thickness or diameter of less than 40 μm, indicating the excellent capability of the FB injector to atomize extremely high viscosity liquids to achieve low-emission combustion.

Acknowledgments This research was supported by the US Department of Energy Award EE0001733.

References

1. Kasabov, P., Zarzalis, N., Habisreuther, P.: Experimental study on lifted flames operated with liquid kerosene at elevated pressure and stabilized by outer recirculation. Flow Turbul. Combust. **90**, 605–619 (2013)
2. Stiehl, R., Schorr, J., Krüger, C., Dreizler, A., Böhm, B.: In-cylinder flow and fuel spray interactions in a stratified spray-guided gasoline engine investigated by high-speed laser imaging technique. Flow Turbul. Combust. **91**, 431–450 (2013)
3. Wright, Y.M., Margari, O.N., Boulouchos, K., Paola, G.D., Mastorakos, E.: Experiments and simulations of n-heptane spray auto-ignition in a closed combustion chamber at diesel engine conditions. Flow Turbul. combust **84**, 49–78 (2010)
4. Bottone, F., Kronenburg, A., Gosman, D., Marquis, A.: The numerical simulation of diesel spray combustion with LES-CMC. Flow Turbul. Combust. **89**, 651–673 (2012)

5. Bhagwan, R., Habisreuther, P.: An experimental comparison of the emissions characteristics of standard jet A-1 and synthetic fuels. Flow Turbulence Combust. doi:10.1007/s10494-014-9528-6
6. Raghavan, V., Rajesh, S., Parag, S., Avinash, V.: Investigation of combustion characteristics of biodiesel and its blends. Combust. Sci. Technol. **181**, 877–891 (2009)
7. Pan, K.L., Li, J.W., Chen, C.P., Wang, C.H.: On droplet combustion of biodiesel fuel mixed with diesel/alkanes in microgravity condition. Combust. Flame **156**, 101926–1936 (2009)
8. Park, S.H., Cha, J., Lee, C.S.: Spray and engine performance characteristics of biodiesel and its blends with diesel and ethanol fuels. Combust. Sci. Technol. **183**, 802–822 (2011)
9. Wang, X., Huang, Z., Kuti, O.A., Zhang, W., Nishida, K.: An experimental investigation on spray, ignition and combustion characteristics of biodiesels. Proc. Combust. Inst. **33**, 2071–2077 (2011)
10. Metzger, B.: Glycerol combustion. M.S. Thesis, Mechanical Engineering Department, North Carolina State University (2007)
11. Bohon, M.D., Metzger, B.A., Linak, W.P., King, C.J., Roberts, W.L.: Glycerol combustion and emissions. Proc. Combust. Inst. **33**, 2717–2724 (2011)
12. Quispe, C.A.G., Coronado, C.J.R., Carvalho Jr. J.A., Linak, W.P., King, C.J., Roberts, W.L.: Glycerol: Production, consumption, prices, characterization and new trends in combustion. Renew Sust. Energ. Rev. **27**, 475–493 (2013)
13. McNeil, J., Day, P., Sirovski, F.: Glycerine from biodiesel: The perfect diesel fuel. Process Saf. Environ. **90**, 180–188 (2012)
14. Queirós, P., Costa, M., Carvalho, R.H.: Co-combustion of crude glycerin with natural gas and hydrogen. Proc. Combust. Inst. **34**, 2759–2767 (2013)
15. Steinmetz, S.A., Herrington, J.S., Winterrowd, C.K., Roberts, W.L., Wendt, J.O.L., Linak, W.P.: Crude glycerol combustion: Particulate, acrolein, and other volatile organic emissions. Proc. Combust. Inst. **34**, 2749–2757 (2013)
16. Simmons, B.M., Agrawal, A.K.: Flow blurring atomization for low-emission combustion of liquid biofuels. Combust. Sci. Technol. **184**, 660–675 (2010)
17. Panchasara, H., Sequera, D., Schreiber, W., Agrawal, A.K.: Combustion performance of a novel injector using flow-blurring for efficient fuel atomization. J. Propul. Power **25**, 984–987 (2009)
18. Sadiki, A., Chrigui, M., Janicka, J., Maneshkarimi, M.R.: Modeling and simulation of effects of turbulence on vaporization, mixing and combustion of liquid-fuel sprays. Flow Turbul. Combust. **75**, 105–130 (2005)
19. Lefebvre, A.H.: Airblast atomization. Prog. Energy Comubst. Sci. **6**, 233–261 (1980)
20. Simmons, B.M., Panchasara, H.V., Agrawal, A.K.: A comparison of air-blast and flow blurring injectors using phase Doppler particle analyzer techniques. P. ASME Turbo Expo. **2**, 981–992 (2009)
21. Pozorski, J., Sazhin, S., Waclawczyk, M., Crua, C., Kennaird, D., Heikal, M.: Spray penetration in a turbulent flow. Flow Turbul. Combust. **68**, 153–165 (2002)
22. Sovani, S.D., Sojka, P.E., Lefebvre, A.H.: Effervescent Atomization. Prog. Energ. Combust. **27**, 483–521 (2001)
23. Panchasara, H.V., Simmons, B.M., Agrawal, A.K.: Combustion performance of biodiesel and diesel-vegetable oil blends in a simulated gas turbine burner. J. Eng. Gas Turb. Power **131**, 1–11 (2009)
24. Simmons, B.M.: Atomization and combustion of liquid biofuels [dissertation]. Tuscaloosa (AL): University of Alabama at Tuscaloosa (2011)
25. Jiang, L., Agrawal, A.K., Taylor, R.P.: Clean combustion of different liquid fuels using a novel injector. Exp. Therm. Fluid. Sci. **57**, 275–284 (2014)
26. Gañán-Calvo, A.M.: Enhanced liquid atomization: From flow-focusing to flow-blurring. Appl. Phys. Lett. **86**, 2141–2142 (2005)
27. Agrawal, S.R., Jiang, L., Agrawal, A.K., Midkiff, K.C.: Analysis of two-phase flow inside a transparent fuel injector. 8th U. S. National Combustion Meeting of the Combustion Institute, Salt Lake City, Utah. Paper No. 070HE-0317 (2013)
28. Simmons, B.M., Agrawal, A.K.: Spray characteristics of a flow blurring atomizer. Atomization Spray **20**, 821–825 (2010)
29. Simmons, B.M., Agrawal, A.K.: Drop size and velocity measurements in bio-oil sprays produced by the flow-blurring injector. P. ASME Turbo Expo. **1**, 701–710 (2011)
30. Jiang, L., Agrawal, A.K., Taylor, R.P.: High speed visualization and PIV measurements in the near field of spray produced by flow-blurring atomization. Accepted by Proc. ASME Turbo Expo 2014: Turbine Technical Conference and Exposition, Düsseldorf, Germany. ASME Paper GT2014-27199 (2014)
31. Keane, R.D., Adrian, R.J.: Theory of cross-correlation analysis of PIV images. Appl. Sci. Res. **49**, 191–215 (1992)
32. Weber, C.: Disintegration of liquid jets. Z. Angew. Math. Mech. **11**, 136–159 (1931)

33. Ohnesorge, W.: Formation of drops by nozzles and the breakup of liquid jests. Z. Angew. Math. Mech. **16**, 355–358 (1936)
34. Lefebvre, A.H.: Atomization and Sprays. Taylor & Francis, NY, USA (1989)
35. Faeth, G.M.: Dynamics of secondary drop breakup- a rate controlling process in dense sprays. Proceedings ILASS-Europe 2002, p. Invited Lecture
36. Batarseh, F.Z.M.: Spray generated by an airblast atomizer: atomization, propagation and aerodynamic instability. Ph.D Thesis, TU Darmstadt, Germany (2008)
37. Jiang, L., Agrawal, A.K.: Combustion of straight glycerol with/without methane using a fuel-flexible, low-emissions burner. Fuel **136**, 177–184 (2014)